

# MISTUNING AND COUPLING EFFECTS IN TURBOMACHINERY BLADINGS

Gerhard Kahl  
*MTU Aero Engines*  
*Munich, Germany*  
Gerhard.Kahl@muc.mtu.de

**Abstract** A numerical method has been developed to study the effects of structural mistuning on the aeroelastic behavior of turbomachinery cascades. The approach used is the combination of a modal reduction technique, where the structural properties of each blade are represented by only a few eigenmodes, with a linearized Euler method for the aerodynamic calculations. The method is validated and applied to two test cases, comprising of a high pressure turbine rotor and a transonic compressor rotor. Both are representative of modern turbomachinery designs. The results of the validation confirm the ability of the present method to accurately capture the dominant effects that influence the aeroelastic behavior of the cascades. Further case studies are performed to assess the influence of alternating and random mistuning on the resonant response amplitudes and on the aeroelastic stability.

## 1. Introduction

Analysis of the aeroelastic behavior of turbomachinery cascades in many cases still rely on the assumption of a perfectly symmetric structure, where all blades are structurally and aerodynamically identical. In practice small differences between the individual airfoils of a cascade are unavoidable. The resulting small variations in the structural characteristics of the individual airfoils can cause dramatic effects. For example, strain gauge tests of complete rotors often show a spread in the measured response amplitudes of the different blades of a factor of more than two. Given the fact that mostly only a few blades are instrumented, this leads to the question what the true maximum amplitude of all blades might be, since this is what the design of the blade has to take into account. Furthermore, the question arises what the effect of the small structural variations on the aeroelastic stability may be, which can often not be measured as readily as the forced response amplitudes.

A wide range of publications exists that assess effects of structural mistuning. However, many of these neglect the aerodynamic damping and coupling altogether (e.g. [1], [2], [9], [14] [11]) or use simplified methods, allowing only for two-dimensional rigid motions of the blade sections [7]. In other instances, the aerodynamic interaction between different structural modes is neglected [13]. The present work puts more emphasis on the aerodynamic damping and coupling effects, while using a simple structural model. The approach presented is intended to allow the consideration of multiple modes for each blade and is capable of dealing with sub- and transonic flow situations. Its main goal is the applicability for design use, meaning that it has to supply results quickly for a large number of configurations.

## 2. Aeroelastic Model

The starting point of this analysis are the fundamental equations of motion in physical space and in the time domain for a discretized system of coupled blades, for example conforming to a FEM approach. For a linear elastic system, these can be formally written as:

$$\tilde{\mathbf{M}}\ddot{\tilde{\mathbf{x}}} + \tilde{\mathbf{D}}\dot{\tilde{\mathbf{x}}} + \tilde{\mathbf{K}}\tilde{\mathbf{x}} + \tilde{\mathbf{F}}_c = \tilde{\mathbf{F}} \quad (1)$$

Here  $\tilde{\mathbf{M}}$ ,  $\tilde{\mathbf{D}}$  and  $\tilde{\mathbf{K}}$  are the mass, damping and stiffness matrices, respectively, while  $\tilde{\mathbf{F}}_c$  introduces the aerodynamic coupling between the blades and is dependent on the deflection and velocity of the blades. The damping is assumed to be of viscous type, i.e. the damping forces are proportional to the velocity. The right hand side,  $\tilde{\mathbf{F}}$  contains the external forces acting on the structure while the vector  $\tilde{\mathbf{x}}$  holds the displacement degrees of freedom for the finite elements of the complete model. For an accurate representation of the vibratory behavior, the number of degrees of freedom (DOF) for a typical cascade will have to be on the order of more than 10,000 times the number of blades. In the present method, a number of assumptions are introduced to arrive at a formulation that is at the same time accurate enough to give a good representation of the true aeroelastic behavior of the structure while still being simple enough to allow rapid analysis of a large number of configurations with variations in the dominant parameters.

The first assumption is that we are dealing with harmonic oscillations of the structure, so that the motion of each blade can be expressed using a complex exponential approach. Furthermore, in order to reduce the number of DOF, a modal approach is employed. It uses a small number  $n_{modes}$  of in-vacuo modeshapes  $\tilde{\Phi}$  of the individual blades as generalized co-ordinates. Thus, each blade of the cascade retains only a few degrees of freedom, which are characterized by the amplitudes  $a_{b,m}$  of the respective modeshapes. While the amplitudes can differ between the individual blades, the underlying modeshapes are as-

sumed to be identical for all blades of the cascade under consideration. The motion  $\tilde{\vec{x}}_b$  of an arbitrary blade  $b$  is then approximated by

$$\tilde{\vec{x}}_b(r, \Phi, z, t) = \vec{x}_b(r, \Phi, z)e^{i\lambda t} = \sum_{m=1}^{n_{modes}} a_{b,m} \vec{\Phi}_m e^{i\lambda t} \quad (2)$$

with

$$\lambda = \omega + i\gamma \quad (3)$$

Here, the complex exponent  $\lambda$  consists of a real part  $\omega$  that represents the angular frequency of oscillation and an imaginary part  $\gamma$  that characterizes the evolution of the amplitude with time, representative of the effective damping present in the system under consideration. In this respect, a positive value of  $\gamma$  implies an exponentially decaying oscillation amplitude, hence positive damping, while a negative value of  $\gamma$  consequently yields exponentially growing amplitudes, corresponding to negative damping, as in the case of a flutter instability. Accordingly, Eq. 1 can be approximated using a reduced set of eigenmodes as

$$[-\lambda^2 \mathbf{M} + i\lambda \mathbf{D} + (\mathbf{K} + \mathbf{C})] \vec{a} = \vec{F} \quad (4)$$

In this equation, only generalized quantities are used. The vector  $\vec{a}$  contains the complex amplitudes for all modes retained for the complete set of blades, hence for an annular cascade consisting of  $n_{blades}$  individual blades, each of which retains  $n_{modes}$  modeshapes, the number of degrees of freedom in this reduced set of equations is  $n_{blades} \cdot n_{modes}$ . The matrix  $\mathbf{D}$  holds the modal damping values that, just like the generalized masses and stiffnesses, can be assigned to each blade and mode individually. While the matrices  $\mathbf{M}$  and  $\mathbf{D}$  are diagonal, the stiffness matrix  $\mathbf{K}$  can contain off-diagonal elements that are used to model mechanical coupling between the individual blades, as it is present through the disk on which the blades are mounted. The vector  $\vec{F}$  in Eq. 4 contains the generalized external forces on the individual blades and modes that result from the projection of the physical forces  $\tilde{\vec{F}}$  on the eigenmodes  $\Phi$  by

$$\vec{F} = \Phi^* \tilde{\vec{F}} \quad (5)$$

Here, the  $\Phi^*$  denotes the hermitian (conjugate-transpose) of the eigenvector matrix  $\Phi$ . Similarly, the aerodynamic coupling forces have been transformed into the modal domain, additionally assuming that a linear aerodynamic approach is valid. Then the modal forces due to the aerodynamic interactions  $\vec{F}_c$  can be written as the product of the complex aerodynamic influence coefficient matrix  $\mathbf{C}$  and the modal amplitudes  $\vec{a}$ :

$$\vec{F}_c = \mathbf{C} \vec{a} = \Phi^* \tilde{\vec{F}}_c \quad (6)$$

The matrix  $\mathbf{C}$ , in contrast to the other matrices, is usually fully populated. It contains the aerodynamic influence coefficients that couple all blades and all modes of the cascade. In the present method, these influence are calculated

using a 3D linearized Euler solver that is an extension of the method described in [5], for further details refer to [6]. Using this reduced model, blade-to-blade variations can be readily introduced into the system by changing the generalized properties mass, stiffness or damping assigned to any of the individual blade modes. Additionally, it is possible to add individually varying or constant mechanical coupling stiffness between different blades.

### Eigenvalue Analysis

In the absence of external forces, the prime interest is on the eigenmodes and eigenvalues of the cascade, describing the flutter stability and the free vibration behavior of the cascade. For this purpose, Eq. 4 can be reformulated as

$$[\mathbf{M}^{-1}(\mathbf{K} + \mathbf{C}) + i\mathbf{M}^{-1}\mathbf{D}\lambda - \mathbf{E}\lambda^2]\vec{a} = \vec{0} \quad (7)$$

Being a non-linear eigenvalue problem, this is fairly inconvenient to solve numerically. To overcome this, it is assumed that the aeroelastic eigenvalues  $\lambda$  do not differ much from the in-vacuo eigenvalues  $\lambda_0$ . Then we can approximate Eq. 7 as

$$[\mathbf{M}^{-1}(\mathbf{K} + \mathbf{C}) + i\mathbf{M}^{-1}\mathbf{D}\lambda_0 - \mathbf{E}\lambda^2]\vec{a} = \vec{0} \quad (8)$$

In this approach, no assumption concerning the distribution of damping in the cascade is made, so that also the effect of damping mistuning can be studied. On the other hand, the approach can only be expected to yield valid results as long as the computed eigenvalues are similar to the in-vacuo eigenvalues of the individual blades. For practical purposes, this condition is usually well met, as discussed in more detail in [6]. To evaluate the aeroelastic stability of a cascade in the presence of aerodynamic and structural coupling as well as structural mistuning, we thus have to solve a linear eigenvalue problem of  $n_{blades} \cdot n_{modes}$  DOF, which can be done very quickly and efficiently with standard numerical solvers even for a large number of mistuned configurations.

### Forced Response Analysis

If external forces are present, then the forced response of the oscillation system is of interest, namely the amplitudes and phases of all the blades after the transients have decayed. For this reason, it is sufficient to set  $\lambda = \omega$  in Eq. 4, because  $\omega$  is now known in advance to be the frequency of the excitation force  $\vec{F}$  and hence is also the oscillation frequency in which the coupled aeroelastic system responds. The resulting linear system of equations

$$[-\omega^2\mathbf{M} + i\omega\mathbf{D} + (\mathbf{K} + \mathbf{C})]\vec{a} = \vec{F} \quad (9)$$

can then be directly solved. In doing so, the appropriate dynamic properties of the individual blades and modes are inserted in the corresponding matrices for any prescribed value of the excitation frequency  $\omega$ .

### 3. Validation: High Pressure Turbine Rotor

The present method was validated using a single stage turbine rig, representative of a modern high-pressure turbine stage. It was designed in the course of the IMT Area 3 turbine project [12] and was used as a cornerstone in various European research programs [8]. In the ADTurB and in the currently running ADTurBII program [4], the main emphasis is on aeroelastic effects. In the ADTurB program, the excitation of the rotor due to the stator wakes was studied, with a special focus on the influence of mechanical mistuning of the rotor blades. The resonant crossing of the 43rd engine order, corresponding to the excitation by the stator wakes, with the 1st torsional eigenmode was studied experimentally in this program. The data gathered in this effort will be used in the following to validate the current method for forced response calculations under mistuned conditions.

The operating point of the test vehicle is slightly transonic with exit Mach numbers just exceeding unity in the stator as well as in the rotor. The eigenfrequencies of all rotor blades were determined by experimental modal analysis with the blades clamped to a massive supporting root block device. It was found that most blades 1T eigenfrequencies clustered around a mean value to within  $\pm 1.5\%$ , while seven blades exhibited significantly lower eigenfrequencies, deviating in excess of 5%. This large deviation was due to the fact that the blades were manufactured in different batches, which resulted in variations of the geometric tolerances and possibly in the properties of the raw material used. As a consequence of this finding, these seven rogue blades were not included to calculate the mean frequency  $f_{mean}$  that is used in the following analysis. The resulting mistuning parameter  $\epsilon = f/f_{mean} - 1$  is shown in fig 1 for every blade, highlighting the severe mistuning of blades 5, 11, 17, 42 and 55 to 57. In the rig experiment, the blades are mounted on a disc, which

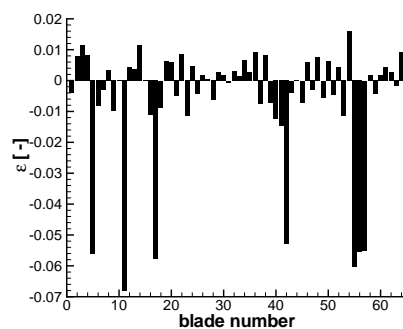


Figure 1. ADTurB rotor 1T mistuning pattern.

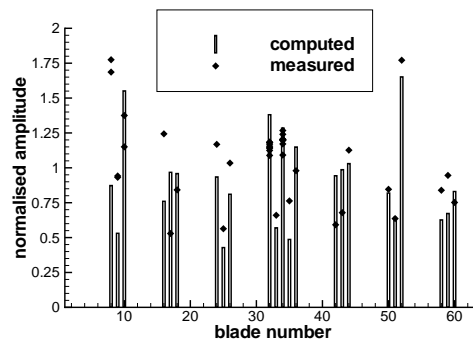


Figure 2. Comparison of computed and measured maximum ADTurB rotor 1T / 43rd EO blade amplitudes.

adds significantly more flexibility to the blade root than the clamping device

of the modal analysis. Furthermore, the disc introduces mechanical coupling between the individual blades. To account for these effects, the generalized stiffness used in the analysis is assumed to be 11% lower than the value resulting from the single blade FE calculation and a coupling stiffness of 0.9% between each two neighboring blades is introduced into the system. These values were deduced from the resonant frequencies measured in the rig test, i.e. after completion of the tests.

Sweeping the excitation frequency through the whole range of interest, the maximum response amplitudes of all blades were computed. A similar procedure was used in the experiment, where the variation of excitation frequency was achieved by speeding up the rotor. This was done sufficiently slowly, so that the influence of transient processes can be neglected. Experimentally determined blade amplitudes are available for 23 of the 64 rotor blades. Fig 2 shows the comparison of the resulting measured and computed maximum response amplitudes for all the blades that have experimental data available. The response amplitudes have been normalized using the mean value of the measured peak amplitudes of all blades.

The measured data for the various blades was taken from a number of different test runs, so that data from more than one run is available for a few of the blades. All the available data is included in this figure, so that the spread of the values for one blade, e.g. blade 32, gives an indication of the repeatability and measurement uncertainty of the experimental data. The figure indicates that the agreement between measured and computed data is quite acceptable. Not only is the mean response amplitude over the whole cascade matched well by the computation, but also the spread between the minimum and the maximum response of any blade is reproduced with good accuracy. Furthermore, in many instances the distribution of the amplitudes to the individual blades is shown by the computation in much the same manner as by the experiments.

To further evaluate the ability of the current method to model the dominant effects of mistuning in this cascade, the amplitude distribution for the complete frequency sweep is compared to experimental values in Fig. 3. Here, the blades 32 through 34 and 36 are chosen for comparison, since the corresponding measured values on these blades were measured simultaneously in a single run, making them particularly well suited for such a comparison. The dashed lines in Fig. 3 indicate the measured values, while the solid lines denote the computed results. The rotor speeds in this figure are non-dimensionalized using the mean measured frequency that was used to determine the values of  $\epsilon$  in Fig. 1.

Comparing the different graphs confirms the good agreement between the computed and the measured maximum amplitudes. Furthermore, the frequency at which this maximum occurs is also well met by the computation. Nevertheless, some significant differences are also visible between the measured and

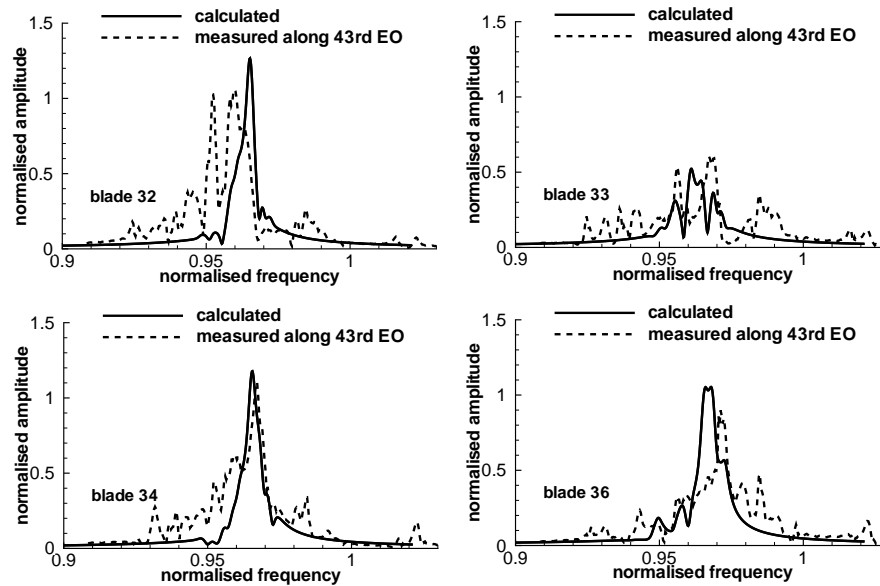


Figure 3. Comparison of computed and measured ADTurB rotor blade 32 to 36 response amplitudes.

the computed results. First, the computed distributions show much smoother curves than the measurements. It is not clear at this point if this behavior can be attributed to stochastic effects in the experiment or if there are deterministic phenomena at work that are not modeled by the current method. Secondly, especially blade number 32 shows two distinct maxima of almost equal magnitude, a fact that is not captured by the computation. In total, it can be concluded that the present method is capable of capturing the essential features of the mistuned cascade and is able to adequately reproduce the dynamic behavior in terms of resonant amplitudes.

#### 4. Case Study: High Pressure Turbine Rotor

In the experimental set-up, only a single arrangement of the blades with their given individual mistuning on the rotor circumference could be studied. From these experiments alone, it is thus not possible to differentiate between the influence of individual blade mistuning and the influence of blade arrangement on the rotor. It remains unclear, whether the specific experimental configuration represents a typical case or - by mere chance - is a rare one with extraordinary high or low amplitudes. Furthermore, from the single configuration studied experimentally, it cannot be shown conclusively whether some correlation between resonant amplitude and mistuning strength exists. To acquire more information on these topics, a further analytical study was performed. Here, 1500 cases were studied, where for each of these the blades were randomly rearranged on the rotor. Each configuration was then analyzed using the same

procedure as described above for the experimental configuration. In Fig. 4, the resulting amplitude values are displayed. Here, the individual maximum blade amplitudes are shown as an interval, where the maximum and minimum for each blade have been marked with the solid gradient and delta symbols, respectively. Note that the blade numbers given here refer to the blades themselves, not to the blade position on the rotor. Each blade number hence corresponds to a single mistuning strength  $\epsilon$ . Further symbols shown in the figure are the solid squares, denoting the median of blade amplitudes for each blade and the open diamonds, showing the computational results for the experimental configuration, as in Fig. 2. The figure shows that the blade relative positioning

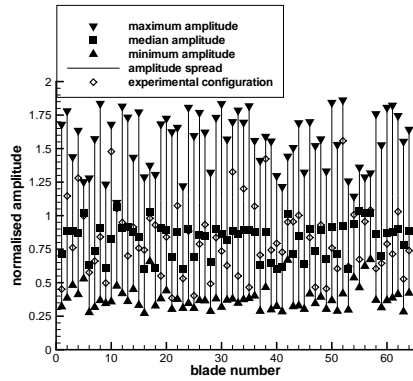


Figure 4. ADTurB rotor 1T / 43rd EO blade amplitudes of each blade over blade number for 1500 configurations of random rearrangement.

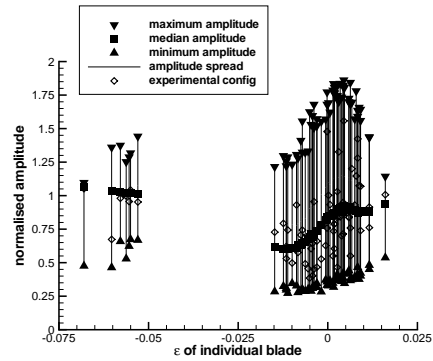


Figure 5. As Fig. 4, but plotted over mistuning parameter  $\epsilon$

around the rotor circumference has a large influence on the response amplitudes. For some blades, the maximum and minimum amplitudes are more than a factor of 5 apart. The median values, representing the highest probability of the amplitudes, however, are restricted to a much smaller band, ranging from normalized amplitude values of approx. 0.6 to 1.1. The values taken from the experimental configuration blend into the range given, covering most of the amplitude region. Furthermore, the distribution of the median values close to normalized amplitudes of 1 indicates that the average of the experimentally observed amplitudes, which was taken as the reference value, is very representative of a typical configuration. Arranging the same data points over the individual blade mistuning parameter  $\epsilon$  results in the graph shown in Fig. 5. Here a certain dependence of the minimum, maximum and median amplitude values on the blade mistuning is apparent. Obviously, the spread of minimum and maximum amplitudes is highest for small positive values of  $\epsilon$ , while it is lower for large negative or positive  $\epsilon$ . The median amplitudes are highest for the blades with large negative mistuning, then drop to significantly lower amplitudes for small negative values of  $\epsilon$  and rise again sharply with small

positive  $\epsilon$ . However, the relative positioning of the blades has a much larger influence on the amplitudes than the individual mistuning strength.

## 5. Case Study: Transonic Compressor Rotor

The second test case studied here is the rotor of a single stage transonic compressor rig [3], representative of a modern HP compressor front stage. It consists of 16 carbon-fiber reinforced rotor blades mounted on a titanium disk and of 29 stator vanes. The tip diameter is 0.38m, maximum relative rotor inlet Mach numbers reach  $Ma_1 = 1.4$  at the tip. At the design speed of 20,000 rpm, the FEM analysis yields the frequencies of 762 Hz for the 1F and of 1505 Hz for the 1T eigenmode. The aerodynamic influence coefficients for the rotor were calculated for these two modes and the aeroelastic eigenvalues were deduced from Eq. 6, assuming a constant mechanical damping (logarithmic decrement) for each mode of  $\delta_{mech} = 0.01$ . The results for a perfectly tuned case are shown in Fig. 6, with the 1F-related eigenvalues on the left and the 1T related ones on the right hand side. The eigenvalues are shown as damping

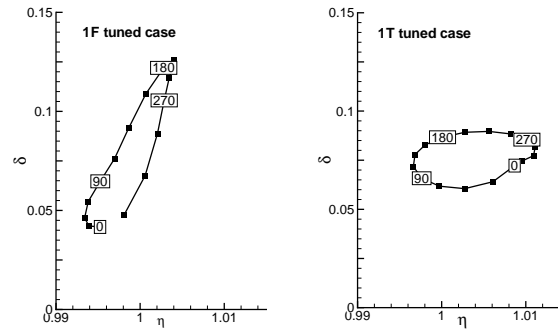


Figure 6. 1T and 1F aeroelastic eigenvalues of the tuned transonic compressor rotor (log. dec.) over frequency ratio  $\eta = f/f_0$  with  $f_0$  being the in-vacu eigenfrequency of the respective modes. For the tuned cascade, the eigenvectors are the well known traveling wave modes with constant interblade phase angle, which is indicated by the inset labels in Fig. 6. The results show that the cascade is aeroelastically stable, all damping values are greater than zero. The damping is in all cases significantly larger than the mechanical damping of  $\delta_{mech} = 0.01$ , indicating that the vibrational behavior of the cascade is dominated by the aerodynamic damping and coupling. Finally, Fig. 6 shows that the eigenfrequencies of the cascade differ up to approximately 1% from the in-vacu eigenfrequency due to the unsteady aerodynamic forces.

In the following, the effects of frequency mistuning are studied on the 1T eigenmode. First, alternating frequency mistuning is introduced, i.e. the generalized stiffness decreased for the odd numbered blades and increased for the even numbered ones. Fig. 7 shows the aeroelastic eigenvalues for the 1T mode. The circles correspond to the tuned configuration, while the triangles

denote the mistuned configuration with a mistuning parameter of  $\epsilon = \pm 0.02$ . Furthermore, the trajectories of the eigenvalues for the values between  $\epsilon = 0$  and  $\epsilon = \pm 0.02$  are indicated by the lines. The results show that the damp-

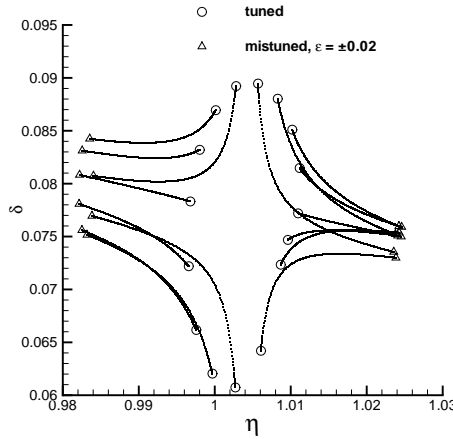


Figure 7. IT aeroelastic eigenvalues of the transonic compressor rotor under alternating mistuning

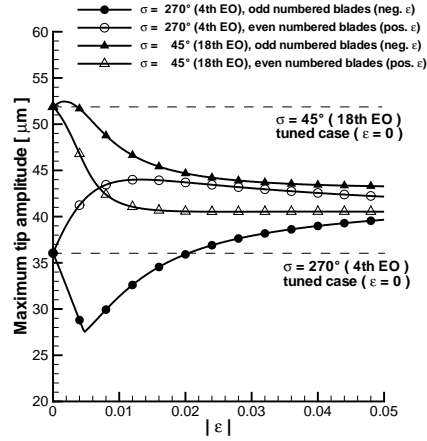


Figure 8. IT resonant amplitudes under alternating mistuning with 4 and 18 EO excitations

ing values converge towards the mean of the tuned configuration values, so that the damping of the least stable eigenvalue is increased, i.e. the cascade is aeroelastically more stable. The alternating mistuning separates the eigenvalues into two distinct clusters, each forming a small ovoid similar to the one of the tuned configuration. This indicates that the blades of equal in-vacuo resonant frequencies are coupled through the unsteady aerodynamic influence coefficients spanning two blade passages, while the immediate neighbors are increasingly decoupled from one another due to their differing structural parameters. When using the same mistuning pattern and applying external excitation forces, the resonant amplitudes arise as shown in Fig. 8. In this figure, the triangles show the situation for a 4 engine order (EO) excitation, the circles denote the response amplitudes for an 18 EO excitation, while open and solid symbols denote the response of the odd and even numbered blades respectively. A first observation from this plot is that the responses for the tuned configuration strongly depends on the EO of the excitation - which is due to the difference in aerodynamic damping, as found in Fig. 6. Furthermore, the resonant responses for the 18 EO excitation decrease with increasing alternating mistuning, while those for the 4 EO excitation increase, at least for the even numbered blades which show the higher amplitudes. This result implies that, in certain cases, deterministic mistuning can be used to decrease the response amplitudes in comparison to the tuned configuration. Finally, the influence of random mistuning on the resonant response has been studied. 500 cases of

randomly generated frequency distributions with the mistuning ranging from  $\epsilon = 0$  to  $\epsilon = \pm 0.25$  have been generated and analyzed for excitation EOs between 0 and 16, corresponding to interblade phase angles of  $\sigma = 0^\circ$  to  $\sigma = 360^\circ$ . In Fig. 9, the resulting maximum response amplitudes are plotted. The figure shows that for excitation interblade phase angles of  $\sigma > 90^\circ$ , all

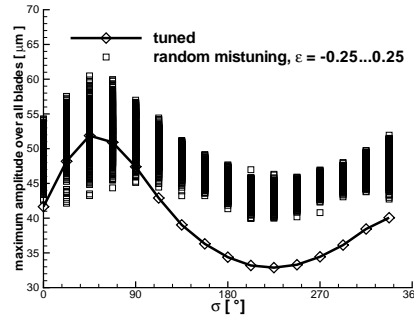


Figure 9. 1T transonic compressor amplitudes under random mistuning.

randomly selected distributions result in larger maximum amplitudes than for the tuned case, while for  $\sigma = 0^\circ$  to  $\sigma = 90^\circ$ , some configurations exist with resulting maximum amplitudes that are lower than for the tuned configuration. The majority of the configurations nevertheless yield higher amplitudes than in the tuned case, in worst mistuned case exceeding the tuned amplitude by more than 40%. It can be observed that the largest relative increase occurs for the excitation interblade phase angle with small tuned response amplitudes and that the spread of the resulting mistuned maximum amplitudes corresponds to the tuned amplitudes for each excitation interblade phase angle: It is small for the cases with small tuned amplitude and large for cases with large tuned amplitudes. Given the fact that the actual configuration of the stochastic mistuning in a real machine cannot be controlled or predicted, it is obvious that the predictions from a tuned cascade model do not yield a conservative value for the resulting maximum amplitudes, but generally produce too low values.

## 6. Summary and Conclusions

A numerical method has been presented that can be used to study the effects of structural mistuning on the aeroelastic behavior of turbomachinery cascades. The method has been validated using data from a recent high pressure turbine experiment and has proven to yield acceptable results in describing the magnitude and distribution of mistuned resonant response amplitudes on the turbine rotor blades. Further case studies on the same turbine rig and on a transonic compressor rig rotor have been performed to demonstrate the multitude of phenomena that can be observed in mistuned aeroelastic systems.

The method presented here has been successfully applied to the modeling of some of these phenomena. Owing to its formulation with only a few degrees

of freedom, it is very fast and thus well suited to perform parametric variations or stochastic "Monte-Carlo" - simulations.

## Acknowledgments

Part of the experimental data used in this thesis was acquired in the research program ADTurB, funded by the European Community under the Industrial and Material Technologies Program (BriteEuRam III), contract no. BPR-CT95-0124. The permission to publish is gratefully acknowledged.

## References

- [1] Afolabi, D.: The Frequency Response of Mistuned Bladed Disk Assemblies, in: *Kielb, R.E. (ed.): Vibrations of Blades and Bladed Disk Assemblies*, pp. 15-22, ASME, 1985.
- [2] Bladh, R.; Castanier, R.; Pierre, C.: Reduced Order Modelling and Vibration Analysis of Mistuned Bladed Disk Assemblies with Shrouds, *Journal of engineering for Gas Turbines and Power*, Vol. 121, pp. 515-522, 1999.
- [3] Blaha, C.; Kablitz, S.; Hennecke, D.K.; Schmidt-Eisenlohr, U.; Pirker, K.; Haselhoff, S.: Numerical Investigation of the Flow in an Aft-Swept Transonic Compressor Rotor, *ASME-GT-0490*, May 2000
- [4] Hennings, H.; Elliot, R.: Forced Response Experiments in a High Pressure Turbine Stage, *ASME-GT-2002-30453*, 2002
- [5] Kahl, G.: Application of a Time Linearized Euler Solver to Aeroelastic Problems in Turbomachinery, *ASME 95-GT-123*, 1995.
- [6] Kahl, G.: Aeroelastic Effects of Mistuning and Coupling in Turbomachinery Bladings, *Communication du Laboratoire Thermique Appliquée et de Turbomachines de l' Ecole Polytechnique Federale de Lausanne*, No. 36, Lausanne, 2002.
- [7] Kielb, R.E.; Kaza, K.R.V.: Effects of Structural Coupling on Mistuned Cascade Flutter and Response, *Trans. ASME J. Eng. Gas Turbines and Power*, Vol. 106, pp. 17-24, Jan. 1984.
- [8] Kost, F.; Hummel, F.; Tiedemann, T.: Investigation of the Unsteady Rotor Flow Field in a Single Stage HP Turbine Stage, *ASME-2000-GT-432*, 2000.
- [9] Moyroud, F.; Fransson, T.; Jaquet-Richardet, G.: A Comparison of Two Finite Element Reduction Techniques for Mistuned Blades, *ASME-2000-GT-0362*, 2000.
- [10] Pierre, C.; Murthy, D.V.: Aeroelastic Modal Characteristics of Mistuned Blade Assemblies: Mode Localization and Loss of Eigenstructure. *AIAA Journal*, Vol. 30, No. 10, pp. 2483-2496, 1992.
- [11] Rivas-Guerra, A.; Mignolet, M.: Local / Global Effects of Mistuning in the Forced Response of Bladed Disks, *ASME-2001-GT-0289*, 2001.
- [12] Santoriello, G.; Colella, A.; Colantuoni, S.: Rotor Blade Aerodynamic Design, Alfa Romeo Avio, IMT Area 3 turbine project technical report, *AER2-CT92-0044*, 1993.
- [13] Seinturier, E.; Lombard, J.-P.; Berthillier, M.; Sgarzi, O.: Turbine Mistuned Forced Response Prediction: Comparison with Experimental Results, *ASME-2002-GT-30424*, 2002.
- [14] Yang, M.-T.; Griffin, J.: A Reduced Order Model of Mistuning Using a Subset of Nominal System Modes, *ASME 99-GT-288*, 1999.